GEOPHYSICS, VOL. 69, NO. 4 (JULY-AUGUST 2004); P. 1046–1052, 7 FIGS.
10.1190/1.1778247

Slowness-weighted diffraction stack for migrating wide-angle seismic data in laterally varying media

Harm J. A. Van Avendonk*

ABSTRACT

Wide-angle prestack depth migration is an important tool for studying the nature of reflecting boundaries in the earth's crust. The slowness-weighted diffraction stack (SWDS) method has been used to incorporate both two-way traveltime constraints and slowness information in the migration. For this purpose, traveltimes and apparent slownesses of reflected arrivals must be calculated in the image space. Earlier applications of SWDS required a 1D or gently varying seismic velocity structure to obtain these quantities by ray tracing in the image space. I show that the apparent slownesses can also be derived directly from one-way traveltime maps using Fermat's principle. The SDWS is applied to an existing onshore–offshore wide-angle data set, and the example shows that the method can be used to image detailed reflectivity structure at great depths.

INTRODUCTION

In the exploration of the structure of the earth's crust, wide-angle seismic reflection–refraction data can provide very good constraints on both seismic velocities and reflecting boundaries in the subsurface. Prestack depth migration is often preferred as a method to investigate the structure of reflecting boundaries (Henstock et al., 1997; Henstock and Levander, 2000). This technique has been applied to wide-angle data using finite-difference methods (Chang and McMechan, 1989; Pilipenko et al., 1999), Kirchhoff integrals (McMechan and Fuis, 1987; Holbrook et al., 1992), and the slowness-weighted diffraction stack (SWDS) (Milkereit, 1987b).

Milkereit (1987b) uses the instantaneous slowness in shot gathers primarily to improve the S/N ratio, although the slowness information also adds directivity to the diffraction stack procedure. Besides satisfying the two-way traveltime condition, the SWDS compares the instantaneous slowness measured in a shot or receiver gather with the slowness of emanating or incoming waves in the model. The use of slowness information in a prestack depth migration is implicit in other techniques such as plane-wave migration (e.g., Temme, 1984; Akbar et al., 1996), but the SWDS gives the user the opportunity to evaluate separately the traveltime and slowness imaging conditions (Tillmanns and Gebrande, 1999). By tuning the window lengths, a local slant stack can be designed to produce a robust measure of instantaneous slowness in the data (Milkereit, 1987a). The slowness constraints are subsequently used in addition to the traveltime imaging condition to focus seismic energy in the image space.

In this paper I present a method that generalizes the SWDS to laterally varying media. This extension is not straightforward, because Milkereit (1987b) uses the ray parameter in 1D kinematic ray-tracing equations as the preferred slowness in his slant stack. Ray shooting can be a computationally expensive method to calculate traveltime maps in laterally varying media. Direct wavefront tracking methods (Vidale, 1990; Moser, 1991; Qin, et al., 1992) are more efficient for calculating traveltimes, but they do not provide the slowness of the incoming or downgoing wavefields. Tillmanns and Gebrande (1999) approach the problem by applying straight-ray migrations (Simon et al., 1996), which allows them to rapidly estimate isochrones and take-off angles in the subsurface. The validity of the straight-ray approximation depends on the amount of velocity heterogeneity in the model, but the effects on the sharpness of a reflection image are potentially severe, particularly if the shallow subsurface is complicated (Peddy et al., 1986). Moreover, in wide-angle studies the reflected waves travel over horizontal distances substantially longer than the reflection depth, such that small imperfections in the seismic velocity model or approximations in the ray-tracing theory can result in defocusing the image.

I propose a method to calculate the slowness of reflected raypaths directly from traveltime maps, with no compromises made regarding the complexity of the seismic velocity model, and I show the effects of slowness weighting on wide-angle migration.

Manuscript received by the Editor September 4, 2001; revised manuscript received August 14, 2003.
*Formerly University of Wyoming, Department of Geology and Geophysics, Laramie, Wyoming; presently University of Texas at Austin, Institute for Geophysics, 4412 Spicewood Springs Road, Austin, Texas 78759. E-mail: harm@ig.utexas.edu.

TRAVELTIME AND APPARENT SLOWNESS

The traveltime condition for prestack depth migration can be visualized by constructing a two-way traveltime map. First, the one-way up- and downgoing traveltime fields must be computed for all sources and receivers, whereby all turning waves are eliminated. Eliminating turning waves is perhaps not straightforward if the eikonal equation is solved to compute traveltime maps, but in the shortest path method the propagation direction is explicitly defined (Moser, 1991). The forward star in the shortest path method (e.g., Moser et al., 1992) can be designed to search only for downgoing paths (Figure 1). The wide-angle migration presented in this paper does not consider underside reflections or reflections from steeply dipping interfaces. Turning waves must therefore be eliminated from the one-way traveltime calculations from both the shots and receivers. To illustrate this adjustment I show shortest path calculations on a grid with large blocks; for other calculations in this paper I use a finer grid. Traveltimes are propagated downward from all sources and receivers in the model, and these one-way traveltime solutions can be summed to construct two-way traveltimes for every source–receiver pair using reciprocity (Figure 2). I perform the shortest path method calculations in this paper in a velocity model constructed from the South Island Geophysical Transect (SIGHT) data set, collected in 1996 across the South Island, New Zealand (Davey et al., 1998; Van Avendonk et al., 1999).

A lack of prior knowledge of the seismic velocity structure and seismic anisotropy can lead to erroneous traveltime maps and a degraded migrated image. The white contour in Figure 2 is the basement depth, which marks a sharp angle in the one-way traveltime contours caused by the large contrast in seismic velocity. In a straightforward application of the diffraction stack, two-way traveltime maps are used to convert the seismic traces from traveltime into the image space by stacking the data along the isochrones. Because of the wide aperture of a wide-angle experiment, two-way traveltime contours span large distances in the image space, indicating a high level of ambiguity in the location of a scattering point. Dip-dependent stacking weights can focus the depth migration in areas where isochrones are not too steep, but stacking weights can also account for the propagation direction of the reflection event. The one-way traveltime maps can also be used to construct apparent slowness maps in the model; these slowness maps can be used to further constrain the migrated image.

Consider two shots S_1 and S_2 that are separated by a small distance ds (Figure 3). An instrument R records reflections from an unknown boundary in the model. The geometrical or minimum traveltime paths bounce from the reflecting interface

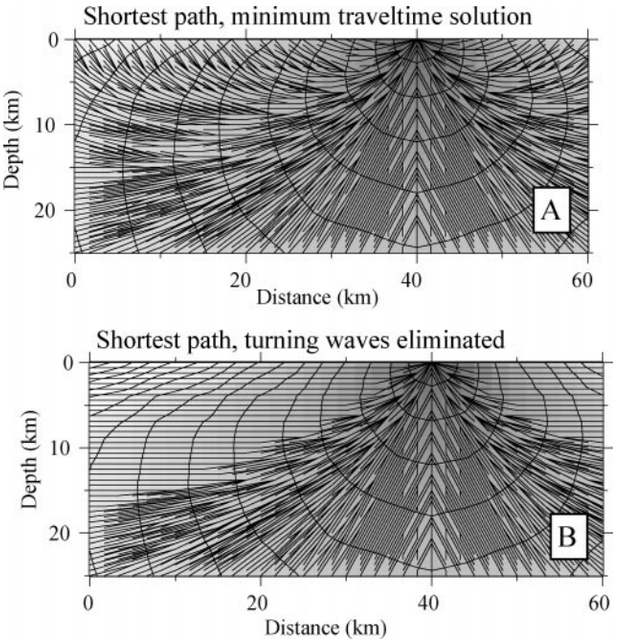

Figure 1. (a) The shortest path method in original form will find minimum traveltime solutions, which include turning waves. The traveltime contours, shown every 1.0 s (thick black lines), are perpendicular to the paths between graph nodes (thin black lines). (b) It is straightforward to restrict the shortest path calculation to downward propagation, but traveltime contours and graph paths are not perpendicular in the distal corners where turning waves have been eliminated.

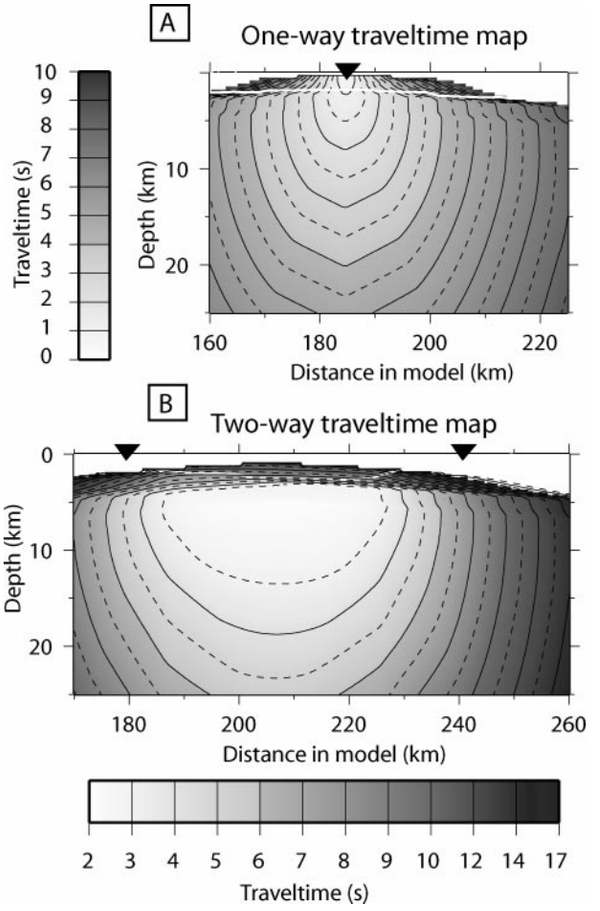

Figure 2. The mapping of seismic reflections in the subsurface relies on accurate traveltime calculations. (a) Downward propagate the traveltimes from the sources and receivers in the seismic velocity model (Van Avendonk et al., 1999). Source and receiver locations: black triangles. Basement: white contour. (b) The two-way traveltime map is constructed by summing the one-way traveltime maps of a source and a receiver. A reduction velocity of 6 km/s in is applied (b). The 3.3-s contour is drawn for comparison with Figures 3 and 4.

at B_1 and B_2. The apparent slowness of the seismic arrival at instrument can be expressed in observed traveltimes and in the take-off angle α of the reflection event:

$$u = \frac{T(S_1, R) - T(S_2, R)}{ds} = \frac{\sin\alpha}{v}, \quad (1)$$

where v is the intrinsic seismic velocity in the medium and $T(S_1, R)$ and $T(S_2, R)$ are the traveltimes from R to S_1 and S_2, respectively. Fermat's principle states that the traveltimes are stationary with respect to small perturbations in these geometrical raypaths. Therefore, the nongeometrical path $S_1 - B_2 - R$ will give approximately the same traveltime as the geometrical path $S_1 - B_1 - R$, provided that ds is much smaller than the length of these paths.

Given that $T(S_1, R)$ in equation (1) can be approximated by the traveltime along the nongeometrical path $S_1 - B_2 - R$, the apparent slowness u can be considered independent of R as long as ds is relatively small:

$$u \approx \frac{T(S_1, B_2) - T(S_2, B_2)}{ds}. \quad (2)$$

Therefore, I can construct a map of apparent slowness by subtracting the one-way traveltime maps (Figure 2a) of nearby shots. The spacing ds between neighboring traveltime maps must be chosen small enough so the near-surface velocity structure does not vary significantly between the two sources, but a very small ds also requires very accurate traveltime calculations to avoid numerical round-off errors in approximation (2). As a compromise I choose $ds = 2$ km for the geometry in this study.

In Figure 4 a map of apparent velocity, the reciprocal of u, is displayed for a pair of surface shots at 181 and 183 km using approximation (2). The apparent velocity of a reflector in the subsurface depends solely on its relative position with respect to the surface shots, regardless of its dip. As expected, the apparent velocity is high beneath the shots, where the rays emanate nearly vertically from the shots, and the apparent velocity approaches the average material velocity in the crust at large distances from the shots.

To illustrate how the traveltime and slowness imaging conditions may complement, I superimpose the 3.3-s two-way traveltime contour for the source–receiver pair in Figure 2b on the apparent velocity map (Figure 4). A seismic sample at 3.3 s from this source–receiver trace must be projected onto this contour to satisfy the traveltime condition. If no slowness information is available, the seismic sample can be stacked along the traveltime contours with dip-dependent weights. A stack weight proportional to $\cos^2\theta$, where θ is the slope of the traveltime isochrones, acts as a simple dip filter in the migration. The dip angle θ is small in wide-aperture seismic study, so the dip-dependent weights will not reduce migration smiles much. However, the apparent velocity varies along the contour from near infinity beneath the shot to 6 km/s near the receiver (Figure 4). The portion of the two-way traveltime contour where the seismic sample is stacked can be restricted if the instantaneous apparent velocity of the data is known.

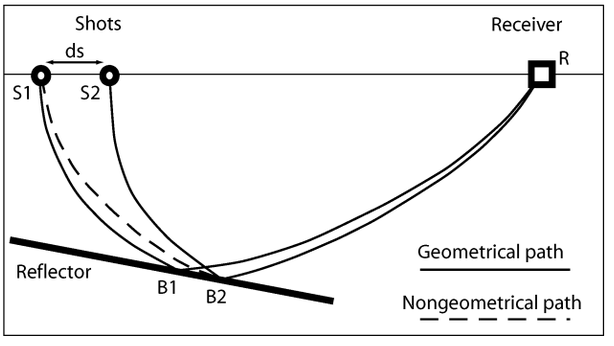

Figure 3. Raypaths for wide-angle reflections recorded by receiver R. The bounce points B_1 and B_2 give minimum traveltimes for shots S_1 and S_2, respectively. The minimum traveltime paths—solid lines; nongeometrical path—dashed line. If the distance ds between the shots is sufficiently small, paths through B_1 and B_2 will produce approximately equal traveltimes between S_1 and S_2.

EXAMPLE OF SLOWNESS WEIGHTING

In a manner similar to (Milkereit, 1987b), I compare the apparent slowness in image space with the instantaneous slowness measured in wide-angle reflection data by a slant stack procedure. The data shown in Figure 5a are taken from an onshore–offshore receiver gather of the SIGHT experiment. Air-gun shots were fired every 50 m along a line in the Tasman Sea with a tuned 8500-in.^{3} (140-liter) array onboard the *R/V Maurice Ewing*. The recording of Figure 5 was made by an onshore instrument on the South Island at a sample rate of 10 ms. The time axis in this figure is reduced by 6 km/s (i.e., a different time delay applied to each trace), such that events with an apparent velocity of 6 km/s are horizontal and events that dip downward to the right have an apparent velocity larger than 6 km/s. The positive seismic amplitudes are shown in gray and black, but the negative amplitudes have been replaced by the instantaneous apparent velocity, shown in the same color scheme as in Figure 4. I define the apparent velocity as the slope in $x - t$ that produces maximum semblance. I calculated

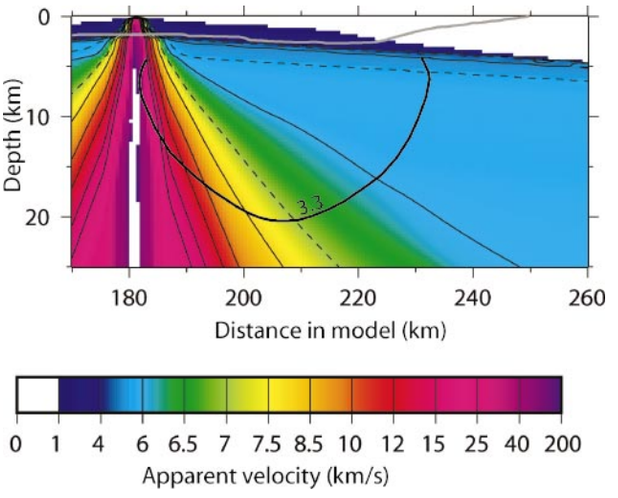

Figure 4. Apparent velocity map in image space calculated by subtracting traveltime maps from two nearby shots at 181 and 183 km. Solid black contours are drawn between 2 and 16 km/s with 2 km/s spacing, and the 3-, 5-, and 7-km/s contours are dashed. The basement is drawn for reference (gray). The apparent velocity of waves traveling vertically from the shots approaches infinity. The 3.3-s two-way traveltime contour of Figure 1b is superimposed to illustrate the variation in apparent velocity along the isochrones.

the semblance w (a value between 0 and 1) by a slant stack in a moving window of 1.2 km by 0.15 s for 25 slownesses between 0.02 and 0.26 s/km. The choice of the size of this window is a trade-off between two competing interests: Semblance measured over a smaller window would be more susceptible to noise, while a considerably larger window would smooth the apparent slowness too much.

Many coherent events are visible in the wide-angle data, but for the purpose of testing the slowness weighting I concentrate on the migration of a midcrustal reflection between 34 and 47 km source–receiver offset (encircled by a heavy dashed line in Figure 5). The observed wide-angle reflection is caused by a prominent velocity discontinuity at a depth of 18 km in the model of Van Avendonk et al. (1999). The event has a dominant apparent velocity of 7.0 to 8.5 km/s. The traveltimes and apparent velocities in Figure 5 can be compared directly with Figures 2 and 4, which use the same receiver location. At 41 km source–receiver offset in Figure 5—the same offset as in Figure 1b—the wide-angle reflection arrives at 3.3 s (thin dashed line), and it has an apparent velocity of ~7.2 km/s. The apparent velocity map shows that this apparent velocity is attained only in a fairly narrow portion of ~10 km along the 3.3-s isochrone (Figure 4).

In the slowness-weighted stack, I apply a weight proportional to $w(u)^2 \cos^2\theta$, where $w(u)$ is the semblance of the seismic data in a slant stack, with slowness u taken from the apparent velocity map of Figure 4. By including directivity in the stacking procedure, smearing along the isochrones is reduced, which results in a sharper reflectivity image. To demonstrate this algorithm, I migrate the midcrustal event in the receiver gather of Figure 4a with and without slowness weighting. A stack with weights that only depend on isochrone dip θ (Figure 6a) shows a few streaks reminiscent of the shape of the two-way traveltime contours, but the amplitude of the migrated reflection is highest where it intersects the prominent boundary in the velocity model of Van Avendonk et al. (1999) (Figure 5b).

The traveltimes of Figure 2 are calculated in a model where this velocity discontinuity was removed, and the coincidence

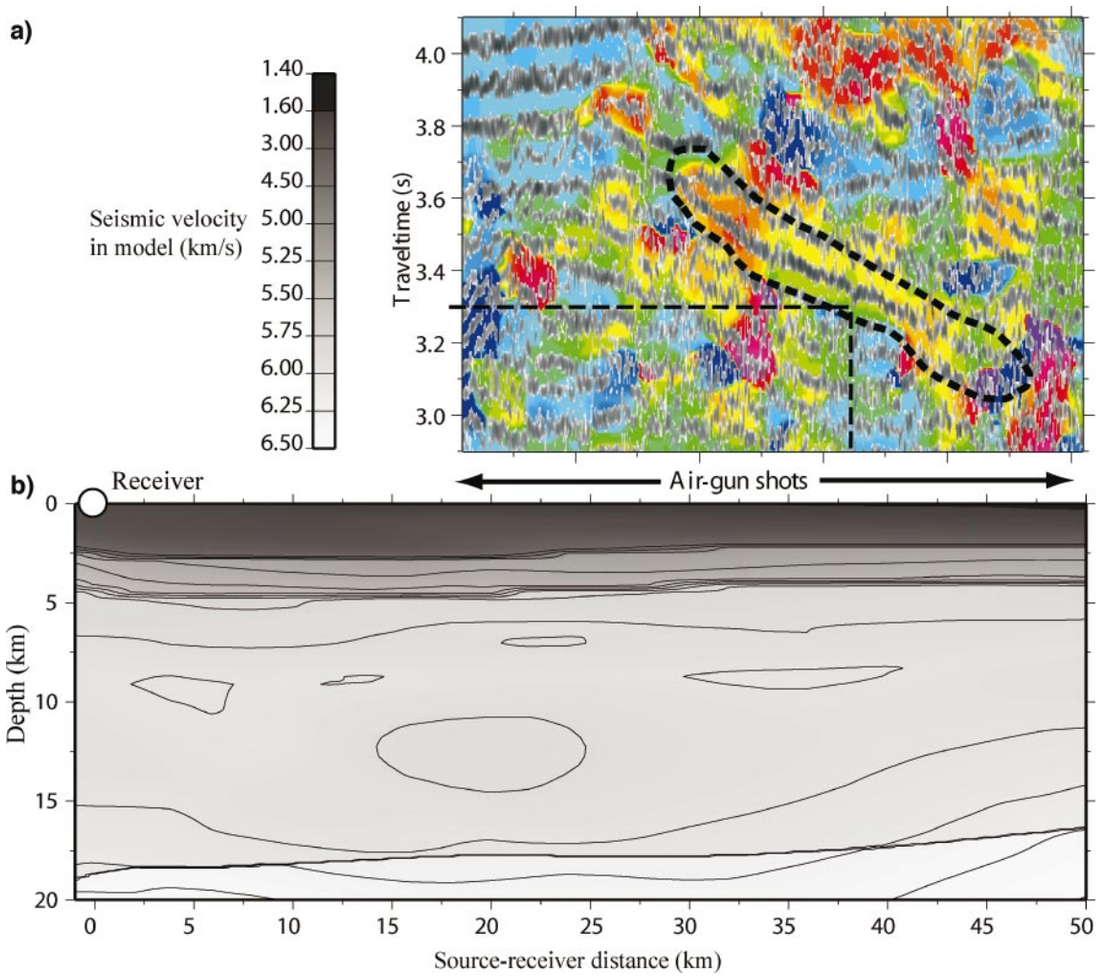

Figure 5. (a) Testing the SWDS on a portion of a receiver gather from the SIGHT project (Davey et al., 1998). The time axis is reduced by 6 km/s. The positive seismic amplitudes are in gray and black, but the negative amplitudes are replaced by the instantaneous apparent velocity. The apparent velocity displayed here produced the maximum semblance in a local slant stack. The seismic reflection arriving at 41 km source–receiver offset (thin dashed line) at 3.3 s is migrated using the traveltime and slowness maps of Figures 2 and 4. (b) The velocity model used in this paper was constructed by traveltime tomography (Van Avendonk et al., 1999).

of the reflectivity structure of Figure 6a with the velocity discontinuity shows the two-way traveltimes are well predicted by the model. It is not desirable to migrate the wide-angle data directly in a seismic velocity model that has large velocity discontinuities because the traveltime maps then become too dependent on the seismic discontinuities that the migration is supposed to illuminate. In Figure 5b slowness weighting is added to the diffraction stack. The SWDS (Figure 6b) produces a higher stack amplitude at the velocity discontinuity than the migration result of Figure 6a.

By stacking data from one receiver gather, we obtain a singlefold stack over a limited distance in model space (Figure 6). Summing the migrated images of neighboring receiver gathers results in a more continuous image of the reflecting boundary (Figure 7). The seven receiver gathers individually produce images of variable quality, but the stack of all these gathers gives a much better picture where these singlefold images overlap. Migration smiles from different gathers do not stack coherently, so the relative amplitude of the imaged velocity discontinuity increases by adding images from several receiver gathers. However, a small left-dipping feature at ~207 km just above the velocity discontinuity is also enhanced by summing migrated receiver gathers. This event cannot be considered an artifact, given that it appears in the same location in most migrated receiver gathers. More likely, the reflection is caused by a dipping fault.

DISCUSSION AND CONCLUSIONS

I have outlined a method for prestack depth migration of wide-angle reflections using detailed seismic velocity information. The method uses both the traveltime and the apparent slowness or dip of observed reflections to migrate them in a seismic velocity model. The calculation of apparent velocities, which are related to take-off angles, requires dense trace spacing. For seismic waves with a dominant frequency of ~10 Hz (Figure 5), a trace spacing of 150 m would be sufficient to avoid aliasing an arrival with an apparent velocity as low as 3 km/s. As can be seen in Figure 4, most wide-angle reflections have apparent velocities between 5 and 10 km/s. Given the good S/N levels, apparent velocities can be measured with high accuracy in marine seismic data, and the shot spacing (50 m in our study) is small enough to avoid aliasing the waves in a receiver gather. In a very dense receiver array such as an ocean-bottom cable, it might even be possible to measure the apparent velocity of an incoming wave in a shot gather.

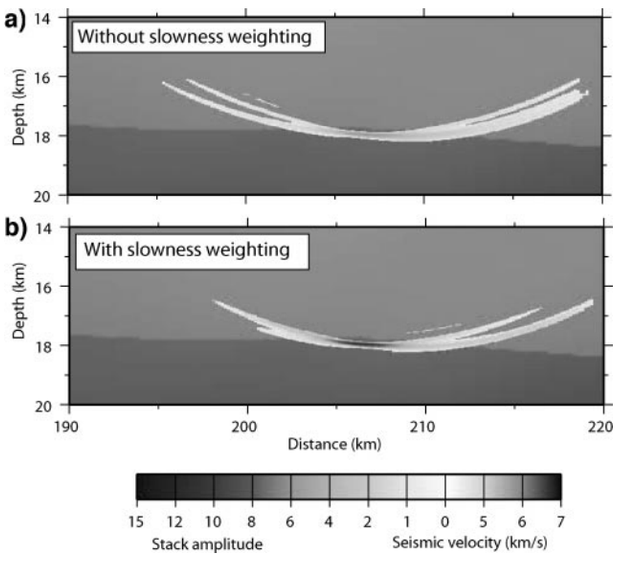

Figure 6. Migration of the reflection highlighted in Figure 5a with (a) a conventional diffractions stack and (b) the SWDS method. Only the positive amplitudes of the reflectivity are shown. Both methods image the reflection at a prominent velocity contrast in the model, but the SWDS (b) produces a more focused image.

The addition of slowness weighting helps to better focus seismic reflections (Figure 6) by summing seismic data over a smaller portion of the isochrones in image space. The wavepath migration (Sun and Schuster, 2001) similarly attempts to restrict the Kirchhoff migration to a Fresnel zone portion of the isochrones. These algorithms can be successful, provided that measurements of apparent slowness or take-off angle are reliable. Other methods that have been used to improve the sharpness of wide-angle migrations are depth focusing (Yilmaz and Chambers, 1984) and residual moveout correction (Lafond and Levander, 1993, 1995). These two approaches do not necessarily require an accurate velocity model, but they are computationally more intensive. The diffraction stack has been used previously to perform amplitude-preserving migrations (Schleicher et al., 1993; Tygel et al., 1993; Hubral et al., 1996). The slowness weighting presented in this paper may help reduce migration smiles, but the SWDS does not preserve reflection amplitude because of the scaling of stack weights with data semblance. An additional practical difficulty with preserving amplitudes in wide-angle migrations would be to account for variations in ground coupling between instruments.

Wide-angle migration has great potential for present and future crustal-scale seismic experiments because the large number of instruments required to record sufficiently dense data sets (Zelt et al., 1998) has become available in recent years. Such data sets (e.g., Davey et al., 1998) also enable us to constrain the detailed seismic velocity structure using reflection tomography (Hole, 1992; Zelt and Smith, 1992; Van Avendonk et al., 2001). An accurate seismic velocity model is necessary to focus deep seismic reflections. Migration schemes that employ accurate ray tracing can successfully image the reflectivity structure in complex geological settings.

Various seismic refractions, reflections, and reverberations are visible in the data shown in Figure 4. By summing seismic energy along isochrones, we assume a single-scattering approximation. For successful application of my algorithm, I must filter or mute out turning waves and multiple reflections. Most of the seismic arrivals with an apparent velocity of less than 6 km/s in Figure 4 are turning waves or the reverberations following refractions. In practice, it is not difficult to selectively migrate portions of the data that are dominated by wide-angle reflections, and the migration of turning waves can therefore be avoided.

As noted by Zelt et al. (1998), reflecting boundaries in the earth's crust can be imaged continuously if the receiver spacing is ~2 km. With the SWDS I have imaged a midcrustal reflecting boundary that was previously modeled in a tomographic inversion (Van Avendonk et al., 1999), but the wide-angle migration also revealed a smaller dipping structure that appeared consistently on a few migrated receiver gathers.

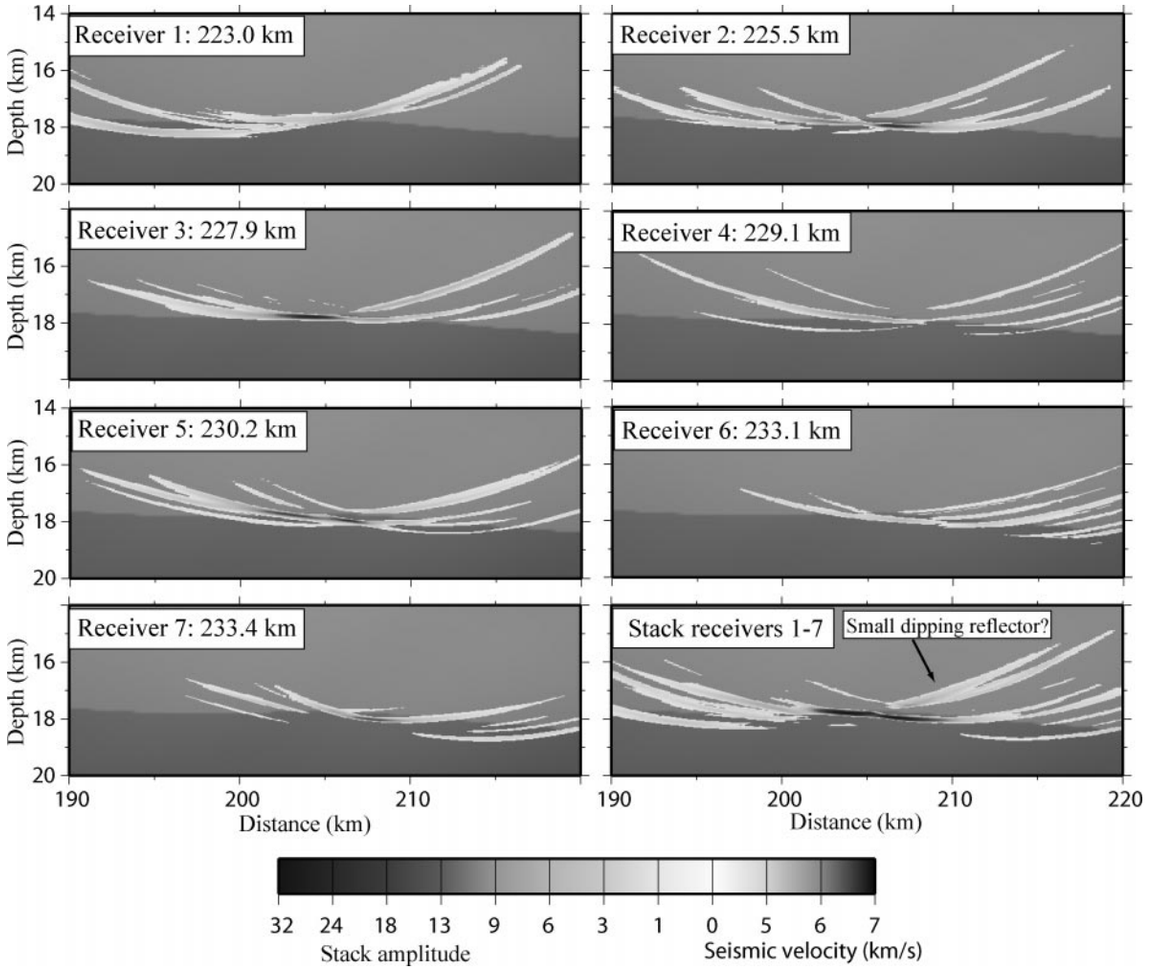

Figure 7. The SWDS method is applied to seven individual receiver gathers, summed in the lower-right image. The full image shows a continuous reflection from the velocity discontinuity modeled by Van Avendonk et al. (1999).

ACKNOWLEDGMENTS

The data used in this paper were collected during the 1996 SIGHT survey. The author thanks all of the U.S. and New Zealand scientists involved in the fieldwork. The research also benefited from discussions with S. Holbrook and D. Okaya. Funding was provided by the U.S. National Science Foundation (EAR-9418530) and the New Zealand Foundation for Research, Science, and Technology.

REFERENCES

Akbar, F. E., Sen, M. K., and Stoffa, P. L., 1996, Prestack plane-wave Kirchhoff migration in laterally varying media: Geophysics, **61**, 1068–1079.

Chang, W.-F., and McMechan, G. A., 1989, Wave field processing of data from the 1986 Program for Array Seismic Studies of the Continental Lithosphere Ouachita experiment: Journal of Geophysical Research, **94**, 17,781–17,792.

Davey, F. J., Henyey, T., Holbrook, W. S., Okaya, D., Stern, T. A., Melhuish, A., Henrys, S., Anderson, H., Eberhart-Phillips, D., Uhrhammer, R., Wu, F., Jiracek, G. R., Wannamaker, P. E., Caldwell, G., and Christensen, N., 1998, Preliminary results from a geophysical study across a modern, continent-continent collisional plate boundary—The Southern Alps, New Zealand: Tectonophysics, **288**, 221–235.

Henstock, T. J., and Levander, A., 2000, Lithospheric evolution in the wake of the Mendocino triple junction: Structure of the San Andreas fault system at 2 Ma: Geophysical Journal International, **140**, 233–247.

Henstock, T. J., Levander, A., and Hole, J. A., 1997, Deformation in the lower crust of the San Andreas fault system in northern California: Science, **278**, 650–653.

Holbrook, W. S., Reiter, E. C., Purdy, G. M., and Toksź, M. N., 1992, Image of the Moho across the continent-ocean transition, U.S. East Coast: Geology, **20**, 203–206.

Hole, J. A., 1992, Nonlinear high-resolution three-dimensional seismic travel time tomography: Journal of Geophysical Research, **97**, 6553–6562.

Hubral, P., Schleicher, J., and Tygel, M., 1996, A unified approach to 3-D seismic reflection imaging, part I: Basic concepts: Geophysics, **61**, 742–758.

Lafond, C. F., and Levander, A. R., 1993, Migration moveout analysis and depth focusing: Geophysics, **58**, 91–100.

——— 1995, Migration of wide-aperture onshore-offshore seismic data, central California: Seismic images of late stage subduction: Journal of Geophysical Research, **100**, 22,231–22,243.

McMechan, G. A., and Fuis, G. S., 1987, Ray equation migration of wide-angle reflections from southern Alaska: Journal of Geophysical Research, **92**, 407–420.

Milkereit, B., 1987a, Decomposition and inversion of seismic data—Instantaneous slowness approach: Geophysical Prospecting, **35**, 875–894.

——— 1987b, Migration of noisy crustal seismic data: Journal of Geophysical Research, **92**, 7916–7930.

Moser, T. J., 1991, Shortest path calculation of seismic rays: Geophysics, **56**, 59–67.
Moser, T. J., van Eck, T., and G. Nolet, 1992, Hypocenter determination in strongly heterogeneous earth models using the shortest path methods: Journal of Geophysical Research, **97**, 6563–6572.
Peddy, C., Brown, L., and Klemperer, S. L., 1986, Interpreting the deep structure of rifts with synthetic seismic sections, *in* Barazangi, M., and Brown, L., Eds., Reflection seismology: A global perspective: American Geophysical Union Geodynamics Series **13**, 301–311.
Pilipenko, V. N., Pavlenkova, N. I., and Luosto, U., 1999, Wide-angle reflection migration technique with an example from the POLAR profile (northern Scandinavia): Tectonophysics, **308**, 445–457.
Qin, F., Luo, Y., Olsen, K. B., Cai, W., and Schuster, G. T., 1992, Finite-difference solution of the eikonal equation along expanding wavefronts: Geophysics, **57**, 478–487.
Schleicher, J., Tygel, M., and Hubral, P., 1993, 3-D true-amplitude finite-offset migration: Geophysics, **58**, 1112–1126.
Simon, M., Gebrande, H., and Bopp, M., 1996, Pre-stack migration and true-amplitude processing of DEKORP near-normal incidence and wide-angle reflection measurements: Tectonophysics, **264**, 381–392.
Sun, H., and Schuster, G. T., 2001, 2-D wavepath migration: Geophysics, **66**, 1528–1537.
Temme, P., 1984, A comparison of common-midpoint, single-shot, and plane-wave depth migration: Geophysics, **49**, 1896–1907.
Tillmanns, M., and Gebrande, H., 1999, Focusing in prestack isochrone migration using instantaneous slowness information: Pure and Applied Geophysics, **156**, 187–206.
Tygel, M., Schleicher, J. Hubral, P., and Hanitzsch, C., 1993, Multiple weights in diffraction stack migration: Geophysics, **59**, 1820–1830.
Van Avendonk, H. J. A., Harding, A. J., Orcutt, J. A., and McClain, J. S., 2001, Contrast in crustal structure across the Clipperton transform fault from travel time tomography: Journal of Geophysical Research, **106**, 10,961–10,981.
Van Avendonk, H. J. A., Holbrook, W. S., Austin, J. K., Okaya, D., and the SIGHT Group, 1999, Seismic velocity and wide-angle reflectivity structure of the Australian-Pacific plate boundary, New Zealand: EOS, **80**, F1029 (abstract).
Vidale, J. E., 1990, Finite-difference calculation of traveltimes in three dimensions: Geophysics, **55**, 521–526.
Yilmaz, O., and Chambers, R., 1984, Migration velocity analysis by wave-field extrapolation: Geophysics, **49**, 1664–1674.
Zelt, B. C., Talwani, M., and Zelt, C. A., 1998, Prestack depth migration of dense wide-angle seismic data: Tectonophysics, **286**, 193–208.
Zelt, C. A., and Smith, R. B., 1992, Seismic traveltime inversion for 2-D crustal velocity structure: Geophysical Journal International, **108**, 16–34.